Cell-derived matrices mechanics as a functional read-out in Collagen VI-related Congenital Muscular Dystrophies

Tom White[a], Arístides López-Márquez[b,c,d,e], Carmen Badosa[b,c,d,e], Cecilia Jiménez-Mallebrera[b,c,d,e], Josep Samitier[a,f,g], Marina I. Giannotti[f,h,i, *], Anna Lagunas[f,a,*]

[a]Nanobioengineering Group, Institute for Bioengineering of Catalonia (IBEC), The Barcelona Institute of Science and Technology (BIST), c/ Baldiri Reixac, 10-12, 08028 Barcelona, Spain.
[b]Laboratorio de Investigación Aplicada en Enfermedades Neuromusculares, Institut de Recerca Sant Joan de Déu, C. de Sta. Rosa, 39, 08950 Barcelona, Spain.
[c]Unidad de Patología Neuromuscular, Servicio de Neuropediatría, Hospital Sant Joan de Déu, Pg. de Sant Joan de Déu, 2, 08950 Esplugues de Llobregat, Barcelona, Spain.
[d]Centro de Investigaciones Biomédicas en Red de Enfermedades Raras (CIBERER), C. de Melchor Fernández Almagro, 3, Fuencarral-El Pardo, 28029 Madrid, Spain.
[e]Department of Genetics, Microbiology and Statistics, Faculty of Biology, University of Barcelona, Diagonal, 643, 08028 Barcelona, Spain.
[f]CIBER-BBN, ISCIII, Barcelona, Spain.
[g]Department of Electronic and Biomedical Engineering, University of Barcelona, Martí Franquès, 1, 08028 Barcelona, Spain.
[h]Nanoprobes & Nanoswitches Group, Institute for Bioengineering of Catalonia (IBEC), The Barcelona Institute of Science and Technology (BIST), c/ Baldiri Reixac, 10-12, 08028 Barcelona, Spain.
[i]Department of Materials Science and Physical Chemistry, University of Barcelona, Martí Franquès, 1, 08028 Barcelona, Spain.

Correspondence to Anna Lagunas (alagunas@ibecbarcelona.eu) and Marina I. Giannotti (migiannotti@ibecbarcelona.eu)

Abstract

Collagen VI-related congenital muscular dystrophies (COL6-RDs) are a set of neuromuscular conditions caused by pathogenic variants found in any of the three COL6 genes. The phenotypic expression of the disease does not directly correlate with the genetic background producing an overlapping spectrum of clinical phenotypes that goes from the mild Bethlem myopathy (BM) to the severe Ulrich congenital muscular dystrophy (UCMD). Diagnosis includes genetic confirmation of the disease and categorization of the phenotype based on maximum motor ability. The development of new tools able to identify phenotype traits can significantly contribute to the diagnosis and prognosis of COL6-RDs. Mutations occurring in COL6 genes result in deficiency or dysfunction of COL6 incorporated into the extracellular matrix (ECM) of connective tissues, affecting its fibrillar structure. Our research group has established personalized pre-clinical models of COL6-RDs based on cell-derived matrices (CDMs), which allowed the direct observation of the fibrillar organization of the ECM in samples derived from patients, and to compare features amongst different phenotypes. Here, we have characterized the mechanical properties of CDMs from patients using atomic force microscopy-based force spectroscopy (AFM-FS). We observed that the elastic modulus (*E*) varies with the phenotype, and that it correlates with COL6 organization in the CDMs. We additionally used AFM-FS to evaluate matrices derived from genetically edited cells, which resulted in *E* value restoration compared to control samples. Altogether, these results anticipate the potential of mechanical analysis of CDMs as a complementary clinical tool, providing phenotypic information about COL6-RDs and their response to gene therapies.

Keywords: atomic force microscopy-based force spectroscopy, collagen-VI related congenital muscular dystrophies, extracellular matrix, cell-derived matrices, elastic modulus, gene editing.

Introduction

Collagen type VI-related congenital muscular dystrophies (COL6-RDs) encompass a heterogenous group of incurable and rare disorders that present different severities of clinical manifestation, assigned based on the initial maximal motor ability [1]. At the milder end of the clinical spectrum, patients with Bethlem myopathy (BM) develop mild weakness in childhood often associated with laxity of distal joints. Prominent contractures typically appear around the age of 10 years and weakness progresses slowly into adulthood resulting in over two-thirds of patients above the age of 50 years losing the ability for ambulation [2]. The phenotype Ulrich congenital muscular dystrophy (UCMD) presents earlier and more severe weakness. Clinical hallmarks including hypotonia, muscle weakness and motor delay appear in the first months of life with patients tending to lose the ability for ambulation between the ages of 5 and 15 years. Deterioration of respiratory function is also a common feature resulting in patients requiring non-invasive ventilation [3]. Although the prevalence of the COL6-RD can only be estimated, given the complex nature of inheritance, a study conducted by the Muscle Centre in Newcastle upon Tyne, England, calculated a prevalence of UCMD as 0.13 cases per 100,000 and a prevalence of BM as 0.77 cases per 100,000 [4]. Whilst these represent the extremes of a clinical continuum, intermediate phenotypes are also expressed where severity cannot easily be classified as either UCMD or BM [5].

Underlying all these forms are mutations in any of the three major collagen VI (COL6) genes, *COL6A1*, *COL6A2*, *COL6A3* [6]. These genes encode three α chains, α1(VI), α2(VI) and α3(VI) respectively, which assemble first to form a triple-helix monomer before further association to dimers and then tetramers via disulfide bond formation. These tetramers are finally secreted in the extracellular matrix (ECM) producing an extended network of beaded microfilaments [7].

The ECM produces an environment for the cell providing physical support as well as regulating cell behavior through different biochemical and physical signals [8]. Key to these functions is the complex composition and organization of different macromolecules within the ECM, which will vary depending on the tissue type [9]. COL6, itself, is thought to perform several key roles including the organization of tissue architecture of skeletal muscles, tendons, bones and cartilage through binding and interaction with different components of the ECM as well as a range of different cytoprotective functions [10].

The composition and structure of the ECM influences its mechanical behavior, which in turn plays a significant role in regulating cell response, generating mechanical forces that stimulate different signaling pathways [11]. As a marker for disease, for example, ECM stiffness alterations have been associated with tumor progression and pulmonary fibrosis [12,13]. Regarding collagen VI deficiency, Bonaldo and collaborators demonstrated that COL6 is fundamental in defining a healthy ECM with a particular stiffness, thus providing the adequate environment for satellite cells (SCs) to regenerate muscle tissue. In a total knockout mouse model (*Col6a1*$^{-/-}$), they observed that muscles are much more elastic than in the wild-type (WT), and that the decrease in stiffness, caused by the lack of COL6 in the ECM, impedes the differentiation of SCs into myoblasts [14].

Recent work in our group has demonstrated that minimalistic preclinical models of ECMs based on cell-derived matrices (CDMs) can be produced using patient COL6-RD dermal fibroblasts [11]. CDMs are natural ECMs assembled by cells resulting in a matrix which closely mimics the *in vivo* stromal fiber organization and molecular content [16–19]. Analysis with Immunofluorescence (IF) and the image processing tool CurveletTransform-Fiber Extraction (CT-FIRE) algorithm enabled reconstruction of single protein fibrils within the CDMs and observed altered arrangement of COL6, Fibronectin (FN) and Fibrillin-1 for COL6-RD patients compared to that of healthy individuals [15]. Based on these previous results and taking advantage of the reductionist model provided by the CDMs, in the present work we use atomic force microscopy-force spectroscopy (AFM-FS) to obtain the young's modulus (*E*) as representative of the stiffness in CDMs from patients diagnosed with

COL6-RDs. We compared the *E* values obtained for the different phenotypes, and with COL6 fibrils morphological features obtained by IF. We further investigate how such AFM-FS studies can be used to evaluate the success of recently developed Nucleic Acid Therapeutic (NAT) treatments, demonstrating the potential of the mechanical analysis of CDMs as a functional biomarker of COL6-RD progression and therapeutic response.

Materials and Methods

Human Fibroblasts

Forearm dermal fibroblasts were used in this study. Dermal fibroblasts were obtained from the Hospital Sant Joan de Deu biobank for five representative COL6-RD patients covering a spectrum of mutations and phenotypes, and two controls unaffected by any neuromuscular condition (Table 1). Primary cells were collected following a standard skin biopsy procedure. All patients had a genetically or pathologically confirmed diagnosis of COL6-RD, with their phenotypes subsequently categorized based on maximum motor ability [1]. Written informed consent was obtained from individuals and/or their parents or guardians. Biological samples were stored and managed by the Hospital Sant Joan de Déu (HSJD) Biobank.

The present study was performed in accordance with the Declaration of Helsinki. All experimental protocols were approved by the Fundació Sant Joan de Déu Ethics Committee on Clinical Research (project identification code: PIC-24-23). Methods were carried out in accordance with relevant guidelines and regulations.

Genetic editing

Results of the editing efficiency are detailed in López-Márquez *et al.* [20]. In summary, CRISPR/*Cas*9-based genome editing was performed on dermal fibroblasts of two patients presenting either the BM (patient 1) or intermediate phenotype (patient 2). Two different CRISPR RNA guides, crRNA_1 (nucleotide sequence: *5'-CCTGGTACCCAACAGGTCTG-3')* and crRNA_2 (nucleotide sequence: *5'-CCCGGGGACCTCAGACCTGT-3')*, were used to silence the dominant-negative *COL6A1* Het. c.877G>A; p.Gly293Arg pathogenic variant present in both individuals, as described [20]. Dermal fibroblast cultures were transfected with the ribonucleoprotein complex formed by the *Cas* 9 endonuclease and the duplex RNA from the union of each of the crRNAs and a fluorescently labeled transactivating crRNA (tracrRNA-ATTO550). Transfection efficiency was measured by fluorescence-activated cell sorting (FACS) using the tracrRNA-ATTO550 fluorophore, resulting in >80% of ATTO550 positive cells for any of the two guides used. Editing success was evaluated by analyzing the DNA reads from transfected cells using Mosaic-Finder [21]. WT *COL6A1* allele resulted almost unaltered, while the mutant allele was reduced more than 50%, demonstrating the specificity of the process. Allele specific expression of *COL6A1* was analyzed by ddPCR using specific probes for WT or mutant cDNA. The normalized expression of the mutant allele was reduced, reaching >80% in Patient 1 treated with crRNA_2 (BM_Edited2). Please refer to the paper from López-Márquez *et al.* [20] for details.

Cell culture

Donor fibroblasts were maintained at 37°C and 5% CO_2 in a high glucose Dulbecco's modified Eagle's Medium (DMEM) (Invitrogen) supplemented with 10% fetal bovine serum (FBS) (Sigma-Aldrich), 1% penicillin and streptomycin (Invitrogen) and 1% sodium pyruvate (Sigma-Aldrich). The growth medium was replaced every 2 days until 80% confluence was reached at which point cells were harvested. To achieve detachment, cells were incubated with 0.25% trypsin-EDTA (Life Technologies) at 37°C and 5% CO_2 for 5 minutes. Supplemented growth medium was then added to inactivate trypsin and the cell suspension was transferred to a 15 ml tube for centrifugation at 500 rpm

for 5 min. The supernatant was discarded, and the pellet resuspended in 10 ml of supplemented growth medium. Using a Neubauer chamber, the number of cells and thus the concentration per ml of suspension could then be calculated for subsequent CDM deposition.

CDM production

CDMs were generated following a previously adapted method in our group [11]. Precleaned glass microscope coverslips (Ø 18 mm, Superior Marienfeld) were incubated with a sterile 1% gelatin (from porcine skin Sigma-Aldrich) solution in PBS (Sigma-Aldrich) at 37°C. A crosslinking reaction for the gelatin layer was initiated with 1% filtered glutaraldehyde in PBS (Sigma-Aldrich) and then quenched with 1 M sterile glycine (Sigma-Aldrich) solution in PBS. The coated coverslips were stored in the fridge with 1% penicillin and streptomycin in PBS for a maximum of two weeks until use.

To produce the CDM, growth medium containing 4 x 10^4 cells/cm^2 of primary fibroblasts was added to the coated substrate. After the fibroblasts had formed a confluent monolayer (approximately 1 day), 50 µg/ml ascorbic acid (AA) in PBS (Sigma-Aldrich) was added every day to stimulate collagen production. Cell media was replaced every three days. After 7 days of AA treatment, samples were decellularized with a filtered extraction buffer: 0.5% Triton X-100 (Sigma-Aldrich) and 300 mM of ammonium hydroxide solution (NH_4OH, Sigma-Aldrich) in PBS. After removal of cell media, this solution was added gently on top of the samples for 4 min before being diluted in 2 ml of PBS. Cell detachment can be monitored under light microscopy [22]. Matrices were stored overnight at 4°C and then washed carefully multiple times to remove any cell debris. To evaluate the effectiveness of the decellularization process, the absence of cellular structures such as cell nuclei was confirmed by IF, as previously described [15].

Immunostaining

CDMs were fixed with formalin 10% (Sigma-Aldrich) for 20 min, before further treatment with ammonium chloride 50 mM (Sigma-Aldrich) in PBS for 20 min to quench any free aldehyde groups. Blocking and permeabilization was then carried out with a solution of 1% bovine serum (BSA) (Sigma-Aldrich) and 0.1% saponin (Sigma-Aldrich) in PBS for 10 min. The matrices were next incubated with the primary antibody mouse monoclonal anti-Collagen VI antibody (Millipore) (1:400) in a PBS solution with 1% BSA and 0.1% saponin for 1 h at room temperature. Samples were carefully rinsed before addition of the fluorophore conjugated secondary antibody: Alexa 488 goat anti-mouse (Thermo Fisher Scientific) (1:1000) in PBS with 1% BS and 0.1% saponin for a further 1 h at room temperature. Nuclei were additionally stained with Hoechst 33342 (Molecular Probes) (1:1000) to ensure successful decellularization (Fig. S1). Samples were finally rinsed with PBS and then mounted with Fluoromount (Sigma-Aldrich) on 76x26 mm microscope slides (RS FRANCE). The samples were allowed to set overnight at room temperature before imaging.

Confocal microscopy

The Zeiss LSM 800 (Carl Zeiss Microscopy GmbH, Jena, Germany) confocal laser scanning microscope with a 20x air (0.8 NA) Plan-Apochromat objective lens was used to acquire 16-bit IF images. Diode lasers with wavelengths 405 and 488 nm were used to excite the relevant fluorophores with emission detection bandwidths configured at 400–500 nm (Hoechst 33342) and 400–570 nm (fluorochrome Alexa 488). Z-stacks were acquired in increments of 1 µm for an average of 20 to reconstruct the 3-dimensionality of the CDM. In total Collagen-VI data was acquired for a minimum of 3 fields of view per replicate with at least two replicates per donor. Laser and detector settings were maintained constant across all samples. Confocal stacks were visualized as maximum intensity

projections using Fiji software [23]. CurveletTransform—Fiber Extraction (CT-FIRE) algorithm was then used to segment individual protein fibrils and calculate biophysical parameters.

AFM-FS

AFM-FS experiments were performed on the decellularized CDMs, at room temperature under liquid environment (PBS buffer solution pH 7.4, 10 mM phosphate, 2.7 mM KCl and 137 mM NaCl). AFM-FS experiments were done with an MFP-3D atomic force microscope (Asylum Research) using a V-shaped Si_3N_4 cantilever with a 10 μm diameter, polystyrene colloidal probe and a nominal spring constant of 0.06 N/m (NOVASCAN). The sensitivity of the photodiode was acquired by recording a deflection-Z position curve on a mica substrate before the cantilever spring constant was calibrated according to the thermal oscillation technique [24]. AFM-FS measurements were performed by approaching and retracting the colloidal probe to the sample at a constant velocity of 3 μm/s, to a maximum applied force around 600 pN. Force-indentation curves were recorded in force map mode acquiring 36 curves within a total scan size of 60 x 60 μm^2. A minimum of 5 distinct sample regions were selected per sample for the force mapping with at least two replicates per donor measured. Measurements were performed on all donors except patient 5 and control 2 (Table 1). The Young's elastic modulus *E* value was determined from these curves by fitting the Hertz model using IGOR Pro 6.22A software to indentation curves (Fig. S4), using a Poisson ratio $\nu = 0.5$, without the need of any correction factor. The fitting was done to a maximum force bellow 400 pN, which ensured an indentation of less than 15% of the sample thickness, estimated to be around 6-10 μm (Fig. S2) [11], thus avoiding any mechanical influence from the underlying substratum [25–28]. Curves were individually analyzed and discarded when excessive adhesion between the sample and tip prevented a good quality of fit for the model.

Statistical Analysis

All statistical analysis and plotting of quantitative data were performed with GraphPad Prism 9. Normality tests were performed before any statistical comparison. For normal distributions, significant differences were assessed with the two-tailed Student's t-test or Tukey's multiple comparisons test for comparison of more than two groups. When data was significantly drawn from a normal distribution, significant differences were assessed with the Mann-Whitney test or Kruskal-Wallis test for comparison of more than two groups. Statistical significance was assumed for $\alpha < 0.05$. At least three replicates per condition and 2 independent experiments were performed in each case (N = 2). When results are grouped together into one phenotype coming from more than one patient it is because there are no significant differences among them.

Results

-CDM fabrication from primary fibroblasts

Human fibroblasts were isolated from forearm skin biopsies of five representative patients covering a spectrum of mutations and phenotypes, and two healthy donors. Their COL6-RD phenotypic classification and genetic background is summarized in Table 1.

Although producing inferior levels of ECM when compared to fibro/adipogenic progenitor cells (FAPs), which are the main ECM source [29–31], dermal fibroblast are readily accessible cells, expandable in culture, expressing high levels of the 3 main COL6 genes [32]. To analyze the composition and mechanical properties of ECMs generated from these cells, personalized CDM models were produced following previous protocols [15,22]. Briefly, confluent cultures of plated fibroblasts were treated with ascorbic acid (AA) for 7 consecutive days stimulating the secretion and inclusion of collagen fibrils. Cellular components were subsequently removed, leaving a 3-dimensional scaffold representative of individual COL6-RD cases (Fig. 1a). The inclusion of COL6 in

the CDMs and the characteristics of COL6 fibers were assessed by IF and image processing through CurveletTransform—Fiber Extraction (CT-FIRE) algorithm (Fig. 1b and S3) [23,33], as previously described [11]. In agreement with results previously reported, a greater number of COL6 fibrils were secreted in control samples, which are also longer and more aligned than in samples from COL6-RD patients.

Table 1. Description of fibroblast donors included in this study with their relevant genetic background.

Donor	Phenotype	Mutation	Gene (pattern of inheritance)	Sex	Age at time of biopsy (years)
Patient 1	BM	c.877G > A (Gly293Arg) Exon 10	*COL6A1* (AD)	Female	9
Patient 2	Intermediate	c.877G > A (Gly293Arg) Exon 10	*COL6A1* (AD)	Male	8
Patient 3	Intermediate	c.2329T > C (Cys777Arg)	*COL6A2* (AD)	Female	12
Patient 4	UCMD	c.901-2A > G Intron 7	*COL6A2* (AD)	Female	3
Patient 5	UCMD	c.930 + 189C > T Intron 11	*COL6A1* (AD)	Male	4
Control 1	-	-	-	Male	1
Control 2	-	-	-	Male	2

Mechanical analysis of CDMs

To evaluate the mechanical properties of the CDMs of the different patients (and phenotypes), we measured the CDM's resistance to deformation and calculated the Young's elastic modulus, *E*. For that, we used AFM-FS, a technique in which a probe consisting of a tip mounted to a microcantilever approaches and indents the sample's surface until a maximum defined force is reached (below 1 nN in this case). At this threshold, the tip is made to retract back to its initial resting position at constant velocity. The interaction forces generated between the tip and sample surface during this cycle are monitored according to the cantilever deflection and this data is used to produce a force-indentation curve [34] (Fig. 1c). Owing to the heterogenous microenvironment of these CDM models, high variability within the same sample can happen for the mechanical response at the nanometer scale. Thus, we selected a spherical geometry (diameter = 10 μm) for the AFM tip to maximize tip-surface contact area and enable the mechanical contribution of multiple matrix fibers to be averaged in a single measurement, to obtain an effective mesoscopic elasticity to compare different samples and conditions, that is more relevant to clinics and diagnostics than that of individual nanoscale components [25,35–37]. Additionally, selecting a spherical tip is advisable for very soft samples, to generate small strains [38].

Force-indentation curves of the different COL6-RDs CDMs displayed clear differences with respect to the contact region response and thus deformability of the matrix (representative curves are shown in Fig. 2a). Before quantification of the CDM's elasticity, the curves were assessed individually to ensure excessive adhesion between the probe and sample was not present. Interestingly, this situation was encountered more frequently for UCMD samples, with many pulling events observed in the retraction curves (Fig. 2a). These are typical patterns for polymeric mesh/network pulling. The Hertz contact model was subsequently applied to the appropriate indentation curves, using *E* as a fitting parameter (Fig. 1c and S4). We found the *E* value for CDM from healthy donors (control) to be 1736 ± 100 Pa, with COL6-RD patients CDMs displaying significant deviations from this 'healthy' range

(Fig. 2b). Whilst an increase in stiffness with *E* of 3313 ± 200 Pa (mean ± SEM) was observed for the intermediate phenotype, CDMs the *E* value was reduced to 659 ± 50 Pa and 152 ± 6 Pa correspondingly for BM and UCMD patients. *E* for Intermediate patients 2 and 3 were not significantly different, with values of 3336 ± 200 Pa and 3019 ± 300 Pa, respectively. Interestingly, a five-fold increase in *E* was calculated for intermediate patient 2 over BM patient 1 CDMs, despite both sharing the same mutant variant. The more frequent observation of pulling events in the BM and, especially, UCMD samples along retraction of the AFM probe (Fig. 2a) suggests a less tight mesh, making it easier to separate and stretch fibers out the ECM.

-CDMs derived from patient fibroblasts genetically edited

CRISPR/*Cas*9-based gene editing was performed on dermal fibroblasts from patients bearing the pathogenic variant *COL6A1* Het. c.877G>A, presenting either the BM (patient 1, Table 1) or intermediate (patient 2, Table 1) phenotype. Two different CRISPR RNA guides, crRNA_1 and crRNA_2 (Fig. 1a), were used to silence the dominant-negative *COL6A1* c.877G>A; p.Gly293Arg pathogenic variant as previously reported [20]. Silencing was demonstrated specific towards the mutant allele, with transcriptional efficacies over 60% for the patients included in the present study, reaching a transcriptional efficacy of >80% for patient 1 treated with crRNA_2 [20]. To examine the response of patient's fibroblasts (patient 1) and (patient 2) to the gene silencing of their mutant allele, CDMs were produced and analyzed following the same IF and nanomechanical protocols previously discussed.

Confocal Analysis of CDMs derived from treated patient fibroblasts

Representative confocal z-projections obtained for COL6 staining in CDMs of the control and COL6-RD samples, produced by edited and unedited cells, are shown in Fig. 3a. Morphological analysis of COL6 fibrils with CT-FIRE shows that gene editing, in general for patient 2 with the intermediate phenotype, and especially when the crRNA_2 guide was used (Edited 2), produces a levelling of the evaluated features towards control values (Fig. 3). Considering COL6 deposition, a significant increase in fibril number, length and width was observed after treatment with either of the two guides used (Fig. 3b-d).

Strikingly, while editing with the crRNA_2 guide statistically levels control values for fibril alignment (Fig. 3e), the use of the crRNA_1 guide does not produce significant differences with respect to the unedited sample. In this regard, López-Márquez et al. also reported variations in patient response as a function of the RNA guide used, with crRNA_2 often recovering more COL6 signal [20].

Alterations in COL6 disposition following treatment of patient fibroblasts were less evident for the BM phenotype. For patient 1, a similar trend to level the control values was observed, especially with cRNA_1-edited samples (Edited 1). However, the increase was found statistically significant only for the number and width of secreted COL6 fibrils.

Mechanical analysis of CDMs derived from treated patient fibroblasts

Markedly, matrices derived from gene-edited cells all obtained values of *E* comparable to the healthy donor (control), independently of the RNA guide used (Fig. 4a). For BM_Edited1 and BM_Edited2, we found the value of *E* to be 1420 ± 90 Pa and 1894 ± 80 Pa (mean ± SEM), respectively, displaying a greater than two-fold increase relative to CDMs from unedited cells of BM patient 1. An increase in compliancy of matrices from the non-treated cells of intermediate patient 2 was additionally achieved, with *E* calculated as 1380 ± 70 Pa considering Intermediate_Edited1 and 1593 ± 100 Pa for Intermediate_Edited2. In all cases, no significant difference between edited samples and the control

(healthy donor) could be highlighted (Fig. 4a). Figure 4b shows representative force-indentation curves for the edited samples.

When the AFM-FS results are compared with the COL6 parameters determined by IF and image processing, the recovery effect of the edited samples towards control values is evident and a healthy range of *E* emerges excluding the different COL6-RD phenotypes (estimated as pale green areas in Fig. 5).

Discussion

COL6-RDs represent a group of neuromuscular disorders affecting the ECM of connective tissues. Patients affected by COL6-RDs produce a lower amount of COL6 with altered assembly and interaction with other components of the ECM [39,40]. Recent studies postulate CDMs as a reductionist *in vitro* model capable of recapitulating the native architecture and composition of the ECM, allowing the identification of the different pathophysiological characteristics of the tissue [41,42]. In a previous study, we demonstrated that CDMs produced from skin fibroblasts of COL6-RD patients exhibit distinctive features compared to those from healthy donor cells, being able to recapitulate the underlying disease. Analyzing secreted COL6 by IF and using curvelet transform-based tools, we found a significantly lower number of assembled COL6 fibers in patient cell-derived matrices, which were also shorter and less aligned compared to those produced by healthy donors [11]. In the present study, we demonstrate how these structural and morphological changes affect the mechanical properties of the CDMs.

The ECM's mechanical response is determined by the organization and relative disposition of its different components [43]. We therefore assessed whether the observed alterations in ECM assembly translate to particular mechanical fingerprints. We obtained the CDMs Young's modulus *E* from force-indentation curves by AFM-FS. We found the stiffness of COL6-RD patient CDMs to deviate significantly from those produced by healthy cells, presenting either an increase or a reduction in *E* depending on the patient. The UCMD phenotype CDMs presented the lowest *E* values. Additionally, pulling events frequently observed in the retraction force curves on UCMD samples suggest a less densely integrated network of fibers. This COL6-RD phenotype associates to earlier and more severe muscle weakness. Interestingly, a softening of the matrix for BM patient 1 compared to intermediate patients (patients 2 and 3) was identified, despite the different phenotype patients 1 and 2 possessing the same pathogenic variant. These differential phenotypic effects likely arise from currently unknown disease modifiers, operating at both genetic and biochemical levels [20].

AFM-FS results agree with those from Bonaldo and collaborators obtained in a total knockout mice model (*Col6a1*-/-), for which a decrease in muscle stiffness was observed due to the lack of COL6 in the ECM [14]. COL6-defficient mice, in general, behave similar to BM phenotypes [44].

Combining results from the IF and mechanical analysis, we are able to identify individuals with COL6-RDs provided with just a skin biopsy. These CDM models may therefore provide a useful diagnostic and prognostic tool to complement current methods, which are mainly focused on motor evaluation.

By using AFM-FS we are able to sense forces at the same scale as mechanoreceptors operating on the surface of cells. Any detected changes to *E*, thus, correspond to those directly perceived by cells, which for alternative macroscopic techniques such as rheometry and tissue stretching would be obscured by the ensemble average of the bulk [25]. Stiffness can produce different mechanical stimuli, which can regulate cell activity both at local and systemic levels through the process of mechanotransduction [45]. As a result, any perturbations to matrix rigidity will generate responses in cells, which could affect their survival, proliferation and migration [46]. Our findings for *E* might therefore help explain impaired processes previously recorded for COL6-RD patients including increased rates in mitochondrial autophagy and apoptosis in skeletal muscle from mice featuring a

knockout of the collagen VI *Col6a1* locus [7], and an accumulation of endosomes-lysosomes and altered mitochondria and Golgi apparatus morphology in primary COL6-RD human fibroblasts [47].

CDMs as testing platform for novel genetic therapies

Whilst no effective treatment is currently available for COL6-RDs, novel NAT have recently emerged as a strategy to target different classes of mutation responsible for the disease [20,32]. The translation of such genetic treatments to the clinic, however, remains difficult owing to underlying heterogeneity of these conditions and need for strategies tailored to an individual's unique biochemical and physiological profile [39]. In order to expand the systematic investigation of these advanced therapies, methods which can evaluate the efficacy of these treatments in a low-cost, quantitative and sensitive manner would therefore be imperative. In the present study we demonstrate how applying the same IF and mechanical analysis to the CDM models provides a promising approach to fill this void.

We tested a CRISPR system recently developed by López-Márquez et al., which was able to silence the mutant allele responsible for substituting glycine 293 for an arginine at the N-terminal in the triple helix of COL6. Two CRISPR RNA guides, namely crRNA_1 and crRNA_2, directed *Cas*9-mediated endonuclease activity to this mutant allele inducing indels, a proportion of which significantly reduced its expression [20].

Matrices derived from gene-edited patient fibroblasts were analyzed in comparison with those produced by the same unedited cells. The IF study of secreted COL6 shows that for the intermediate phenotype patient there is a recovery of the values of the different characteristics evaluated, towards the control values, especially when using the crRNA_2 guide (Edited 2). However, although the same trend is intuited for the BM phenotype, significant differences were only found for the number of fibrils and their width in the crRNA_1-edited samples (Edited 1). This is in agreement with previous results of López-Márquez et al., achieving higher percentage increases of COL6 intensity in the ECMs of the edited intermediate phenotypes [20].

From AFM-FS studies, we demonstrate how fiber organization affects matrix stiffness and that it is possible to define a healthy range of *E* that excludes the different COL6-RD phenotypes. After genetic correction, the stiffness determined for patient matrices does not show significant differences with respect to control CDMs (healthy donors), suggesting a restoration of ECM mechanical properties, regardless of the phenotype or crRNA guide used. This would indicate that the analysis of samples by AFM-FS is able to detect the changes produced by gene editing with a higher sensitivity than IF combined with image analysis, thus highlighting the mechanical characteristics of the matrix as a sensitive biomarker [48] for the assessment of NAT applied to COL6-RDs.

Overall, these results support the application of CRISPR/*Cas* 9 for COL6-RDs treatment, and CDMs as adequate *in vitro* models for their testing. In addition, mechanistic analysis of patient CDMs by AFM-FS provides a functional readout to help assign a value to pathogenic variants and monitor therapies, thus complementing current diagnostic tools.

However, some limitations of the present study should be acknowledged. Since it is limited to a small number of patients, it is not possible to predict the real clinical significance, for which the evaluation of a larger cohort would be necessary. Structural characterization, moreover, has focused on COL6, without including other matrix components that could also have relevant implications. Due to the "personalized" nature of these models with the biological variability of each individual patient, a more generalized view of the study would require the inclusion of different mutations and phenotypic expressions.

In conclusion, changes to the mechanical properties of CDMs derived from patient fibroblasts are observed in this study and related to the alterations in protein assembly associated with COL6-RDs. Variations in the stiffness reflect not only their specific mutation but also the cascade of events that

lead to the final phenotypic expression. Additionally, we illustrate how the CDMs can provide a preliminary testing platform for novel genetic therapies. The response of different patient cells to a recently developed CRISPR/*Cas* 9 gene correction strategy was assessed and a recovery in deposited COL6 as well restoration in matrix stiffness was observed. We envision that these *in-vitro* models will ultimately help translate new therapeutic findings to clinical practice.

CRediT authorship contribution statement

A. Lagunas: Conceptualization, Methodology, Formal analysis, Writing – Original Draft, Visualization, Writing – Review & Editing, Supervision, Project administration, Funding acquisition. **M. I. Giannotti:** Conceptualization, Methodology, Formal analysis, Writing – Original Draft, Visualization, Writing – Review & Editing, Supervision, Project administration, Funding acquisition. **C. Jiménez-Mallebrera:** Methodology, Resources (obtention of patient samples), Supervision, Writing – Review & Editing, Project administration, Funding acquisition. **J. Samitier:** Conceptualization, Writing – Review & Editing, Supervision, Project administration, Funding acquisition. **C. Badosa:** Methodology, Investigation, Writing – Review & Editing. **T. White:** Methodology, Investigation, Formal analysis, Visualization, Writing – Original Draft. **A. López-Márquez:** Methodology, Investigation, Resources (gene editing), Formal analysis, Writing – Review & Editing.

Declaration of competing interest

The authors declare no competing interests.

Data availability

Data will be made available on request.

Acknowledgements

We acknowledge M. Funes, M. Pérez and E. Almici for technical support and F. S. Tedesco for fruitful discussions. We also acknowledge the Advanced Digital Microscopy Unit at the Institute for Research in Biomedicine (IRB Barcelona). We thank the Nanometric Techniques Unit from the Scientific and Technological Centers of the University of Barcelona (CCiT-UB) for technical assistance. We are grateful to Fundación Noelia for their support to the Jimenez-Mallebrera´s lab at IRSJD and the Biobank HSJD. We acknowledge all the individuals and their families for their support, collaboration, and encouragement. We are indebted to the Biobank of the Hospital Sant Joan de Déu.

Financial support from “Plan Complementario de Biotecnología aplicada a la Salud”, coordinated by Institute for Bioengineering of Catalonia (IBEC) within the framework of “Plan de Recuperación, Transformación y Resiliencia (C17.I1) – financed by the European Commission – NextGenerationEU”. Financial support from Spanish Ministry of Science and Innovation (project PID2022-140459OB-I00 funded by MCIN/AEI/10.13039/501100011033/ and by FEDER A way of making Europe), Department of Research and Universities of the Generalitat de Catalunya (2021 SGR 01545, 2021 SGR 01410), Instituto de Salud Carlos III (ISCIII, grants PI19/0122 and PI22/01382), CERCA Programme / Generalitat de Catalunya, and Networking Biomedical Research Center (CIBER) of Spain. CIBER is an initiative funded by the VI National R&D&i Plan 2008-2011, Iniciativa Ingenio 2010, Consolider Program, CIBER Actions and the Instituto de Salud Carlos III, with the support of the European Regional Development Fund (ERDF).

Ethical disclosure

The authors state that they have obtained appropriate institutional review board approval and have followed the principles outlined in the Declaration of Helsinki for all human experimental investigations. Written informed consent was obtained from individuals and/or their parents or guardians. Biological samples were stored and managed by the Hospital Sant Joan de Déu (HSJD) Biobank.

Fig./Table legends

Table 1. Description of fibroblast donors included in this study with their relevant genetic background.

Figure 1. Preparation and analysis workflow for CDMs. **a)** CDMs production: Confluent cultures of primary fibroblasts were treated with ascorbic acid (AA) for 7 days to stimulate collagen synthesis and secretion in the ECM. Decellularization was then performed using a mild alkaline surfactant to solubilize cytoplasmic components and disrupt protein and lipid interactions. Nucleic acid therapy (NAT) on patients' dermal fibroblasts was conducted by CRISPR/*Cas*9 gene silencing of the pathogenic allele using two different RNA guides crRNA_1 and crRNA_2. **b)** Analysis was performed with IF staining for COL6 to evaluate the composition and morphology of the ECM and **c)** subsequent AFM-FS studies on the produced CDMs enabled the assessment of the matrix stiffness.

Fig. 2. Mechanical analysis of CDMs. **a)** Representative force-indentation curves for each condition tested (dark: approach, light: retraction). **b)** Values of the Young's modulus (*E*) for CDMs obtained from healthy donors (control) and COL6 RD patient cells: Intermediate (patients 2 and 3), BM (patient 1) and UCDM (patient 4) phenotypes. Results (bars graphs) are the mean ± SD. ****$p < 0.0001$, ns = no significant difference.

Fig. 3. Effect of gene editing on COL6 deposition in CDMs. **a)** Representative confocal z-projections of immunostained COL6 (trimeric form) in the CDMs: from fibroblasts of healthy donors (Control) and from COL6-RD patients 1 and 2 with BM and intermediate phenotypes, respectively, before and after gene editing using either crRNA_1 (Edited1) or crRNA_2 (Edited2). Scale bar = 50 µm. **b-e)** Graphs displaying various characteristics of COL6 fibrils obtained by image processing with CT-FIRE algorithm. Results are the mean ± SD. *$p < 0.05$, **$p < 0.01$, ***$p < 0.001$ ****$p < 0.0001$.

Fig. 4. Mechanical analysis of CDMs derived from edited COL6-RD patient fibroblasts. **a)** Values of the Young's modulus (*E*) for CDMs from fibroblasts of healthy donors (Control) and from COL6-RD patients 1 and 2 with BM and intermediate phenotypes, respectively, before and after gene editing using either crRNA_1 (Edited1) or crRNA_2 (Edited2). Results (bars graphs) are the mean ± SD. ****$p < 0.0001$, ns = no significant difference. **b)** Representative force-indentation curves for CDMs from COL6-RD patients 1 and 2 with BM and intermediate phenotypes, respectively, using either crRNA_1 (Edited1) or crRNA_2 (Edited2) (dark: approach, light: retraction).

Fig. 5. Correlation between structural and mechanical characteristics. **a)** Representation of the COL6 parameters determined by IF and image processing against the CDM's stiffness (Young's modulus) measured by AFM-FS. The pale green areas represent the recovery towards control values in the edited samples.

References

[1] D. Natera-de Benito, A.R. Foley, C. Domínguez-González, C. Ortez, M. Jain, A. Mebrahtu, S. Donkervoort, Y. Hu, M. Fink, P. Yun, T. Ogata, J. Medina, M. Vigo, K.G. Meilleur, M.E. Leach, J. Dastgir, J. Díaz-Manera, L. Carrera-García, J. Expósito-Escudero, M. Alarcon, D. Cuadras, E. Montiel-Morillo, J.C. Milisenda, R. Dominguez-Rubio, M. Olivé, J. Colomer, C. Jou, C. Jimenez-Mallebrera, C.G. Bönnemann, A. Nascimento, Association of Initial Maximal Motor Ability With Long-term Functional Outcome in Patients With COL6-Related Dystrophies, Neurology 96 (2021) e1413–e1424. https://doi.org/10.1212/WNL.0000000000011499.

[2] G.J. Jöbsis, J.M. Boers, P.G. Barth, M. de Visser, Bethlem myopathy: a slowly progressive congenital muscular dystrophy with contractures, Brain 122 (Pt 4) (1999) 649–655. https://doi.org/10.1093/brain/122.4.649.

[3] C.G. Bönnemann, The collagen VI-related myopathies: muscle meets its matrix, Nat Rev Neurol 7 (2011) 379–390. https://doi.org/10.1038/nrneurol.2011.81.

[4] F.L.M. Norwood, C. Harling, P.F. Chinnery, M. Eagle, K. Bushby, V. Straub, Prevalence of genetic muscle disease in Northern England: in-depth analysis of a muscle clinic population, Brain 132 (2009) 3175–3186. https://doi.org/10.1093/brain/awp236.

[5] A.R. Foley, P. Mohassel, S. Donkervoort, V. Bolduc, C.G. Bönnemann, Collagen VI-Related Dystrophies, in: M.P. Adam, G.M. Mirzaa, R.A. Pagon, S.E. Wallace, L.J. Bean, K.W. Gripp, A. Amemiya (Eds.), GeneReviews®, University of Washington, Seattle, Seattle (WA), 1993. http://www.ncbi.nlm.nih.gov/books/NBK1503/ (accessed July 7, 2023).

[6] A. Lampe, K. Bushby, Collagen VI related muscle disorders, J Med Genet 42 (2005) 673–685. https://doi.org/10.1136/jmg.2002.002311.

[7] P. Bernardi, P. Bonaldo, Dysfunction of mitochondria and sarcoplasmic reticulum in the pathogenesis of collagen VI muscular dystrophies, Ann N Y Acad Sci 1147 (2008) 303–311. https://doi.org/10.1196/annals.1427.009.

[8] R.P. Mecham, Overview of extracellular matrix, Curr Protoc Cell Biol Chapter 10 (2001) Unit 10.1. https://doi.org/10.1002/0471143030.cb1001s00.

[9] J.K. Mouw, G. Ou, V.M. Weaver, Extracellular matrix assembly: a multiscale deconstruction, Nat Rev Mol Cell Biol 15 (2014) 771–785. https://doi.org/10.1038/nrm3902.

[10] M. Cescon, F. Gattazzo, P. Chen, P. Bonaldo, Collagen VI at a glance, Journal of Cell Science 128 (2015) 3525–3531. https://doi.org/10.1242/jcs.169748.

[11] R.G. Wells, The role of matrix stiffness in regulating cell behavior, Hepatology 47 (2008) 1394–1400. https://doi.org/10.1002/hep.22193.

[12] K. Jandl, G. Kwapiszewska, Stiffness of the Extracellular Matrix: A Regulator of Prostaglandins in Pulmonary Fibrosis?, Am J Respir Cell Mol Biol 63 (2020) 721–722. https://doi.org/10.1165/rcmb.2020-0398ED.

[13] E.V. Petersen, D.A. Chudakova, E.Yu. Skorova, V. Anikin, I.V. Reshetov, O.A. Mynbaev, The Extracellular Matrix-Derived Biomarkers for Diagnosis, Prognosis, and Personalized Therapy of Malignant Tumors, Front Oncol 10 (2020) 575569. https://doi.org/10.3389/fonc.2020.575569.

[14] A. Urciuolo, M. Quarta, V. Morbidoni, F. Gattazzo, S. Molon, P. Grumati, F. Montemurro, F.S. Tedesco, B. Blaauw, G. Cossu, G. Vozzi, T.A. Rando, P. Bonaldo, Collagen VI regulates satellite cell self-renewal and muscle regeneration, Nat Commun 4 (2013) 1964. https://doi.org/10.1038/ncomms2964.

[15] E. Almici, V. Chiappini, A. López-Márquez, C. Badosa, B. Blázquez, D. Caballero, J. Montero, D. Natera-de Benito, A. Nascimento, M. Roldán, A. Lagunas, C. Jiménez-Mallebrera, J. Samitier, Personalized in vitro Extracellular Matrix Models of Collagen VI-Related Muscular Dystrophies, Frontiers in Bioengineering and Biotechnology 10 (2022). https://www.frontiersin.org/articles/10.3389/fbioe.2022.851825 (accessed July 7, 2023).

[16] M.L. Kutys, A.D. Doyle, K.M. Yamada, Regulation of cell adhesion and migration by cell-derived matrices, Experimental Cell Research 319 (2013) 2434–2439. https://doi.org/10.1016/j.yexcr.2013.05.030.

[17] A.D. Doyle, F.W. Wang, K. Matsumoto, K.M. Yamada, One-dimensional topography underlies three-dimensional fibrillar cell migration, Journal of Cell Biology 184 (2009) 481–490. https://doi.org/10.1083/jcb.200810041.

[18] J.G. Goetz, S. Minguet, I. Navarro-Lérida, J.J. Lazcano, R. Samaniego, E. Calvo, M. Tello, T. Osteso-Ibáñez, T. Pellinen, A. Echarri, A. Cerezo, A.J.P. Klein-Szanto, R. Garcia, P.J. Keely, P. Sánchez-Mateos, E. Cukierman, M.A. Del Pozo, Biomechanical Remodeling of the Microenvironment by Stromal Caveolin-1 Favors Tumor Invasion and Metastasis, Cell 146 (2011) 148–163. https://doi.org/10.1016/j.cell.2011.05.040.

[19] J.-E.W. Ahlfors, K.L. Billiar, Biomechanical and biochemical characteristics of a human fibroblast-produced and remodeled matrix, Biomaterials 28 (2007) 2183–2191. https://doi.org/10.1016/j.biomaterials.2006.12.030.

[20] A. López-Márquez, M. Morín, S. Fernández-Peñalver, C. Badosa, A. Hernández-Delgado, D. Natera-de Benito, C. Ortez, A. Nascimento, D. Grinberg, S. Balcells, M. Roldán, M.Á. Moreno-Pelayo, C. Jiménez-Mallebrera, CRISPR/Cas9-Mediated Allele-Specific Disruption of a Dominant COL6A1 Pathogenic Variant Improves Collagen VI Network in Patient Fibroblasts, International Journal of Molecular Sciences 23 (2022) 4410. https://doi.org/10.3390/ijms23084410.

[21] A. Fernández, M. Morín, D. Muñoz□Santos, S. Josa, A. Montero, M. Rubio□Fernández, M. Cantero, J. Fernández, M.J. Del Hierro, M. Castrillo, M.Á. Moreno□Pelayo, L. Montoliu, Simple Protocol for Generating and Genotyping Genome□Edited Mice With CRISPR□Cas9 Reagents, CP Mouse Biology 10 (2020) e69. https://doi.org/10.1002/cpmo.69.

[22] R. Kaukonen, G. Jacquemet, H. Hamidi, J. Ivaska, Cell-derived matrices for studying cell proliferation and directional migration in a complex 3D microenvironment, Nat Protoc 12 (2017) 2376–2390. https://doi.org/10.1038/nprot.2017.107.

[23] J. Schindelin, I. Arganda-Carreras, E. Frise, V. Kaynig, M. Longair, T. Pietzsch, S. Preibisch, C. Rueden, S. Saalfeld, B. Schmid, J.-Y. Tinevez, D.J. White, V. Hartenstein, K. Eliceiri, P. Tomancak, A. Cardona, Fiji: an open-source platform for biological-image analysis, Nat Methods 9 (2012) 676–682. https://doi.org/10.1038/nmeth.2019.

[24] R. Proksch, T.E. Schäffer, J.P. Cleveland, R.C. Callahan, M.B. Viani, Finite optical spot size and position corrections in thermal spring constant calibration, Nanotechnology 15 (2004) 1344. https://doi.org/10.1088/0957-4484/15/9/039.

[25] J. Otero, D. Navajas, J. Alcaraz, Chapter 4 - Characterization of the elastic properties of extracellular matrix models by atomic force microscopy, in: D. Caballero, S.C. Kundu, R.L. Reis (Eds.), Methods in Cell Biology, Academic Press, 2020: pp. 59–83. https://doi.org/10.1016/bs.mcb.2019.11.016.

[26] V. Vyas, M. Solomon, G.G.M. D'Souza, B.D. Huey, Nanomechanical Analysis of Extracellular Matrix and Cells in Multicellular Spheroids, Cel. Mol. Bioeng. 12 (2019) 203–214. https://doi.org/10.1007/s12195-019-00577-0.

[27] J. Alcaraz, J. Otero, I. Jorba, D. Navajas, Bidirectional mechanobiology between cells and their local extracellular matrix probed by atomic force microscopy, Seminars in Cell & Developmental Biology 73 (2018) 71–81. https://doi.org/10.1016/j.semcdb.2017.07.020.

[28] N. Gavara, R.S. Chadwick, Determination of the elastic moduli of thin samples and adherent cells using conical atomic force microscope tips, Nature Nanotech 7 (2012) 733–736. https://doi.org/10.1038/nnano.2012.163.

[29] A.W.B. Joe, L. Yi, A. Natarajan, F. Le Grand, L. So, J. Wang, M.A. Rudnicki, F.M.V. Rossi, Muscle injury activates resident fibro/adipogenic progenitors that facilitate myogenesis, Nat Cell Biol 12 (2010) 153–163. https://doi.org/10.1038/ncb2015.

[30] A. Uezumi, S. Fukada, N. Yamamoto, S. Takeda, K. Tsuchida, Mesenchymal progenitors distinct from satellite cells contribute to ectopic fat cell formation in skeletal muscle, Nat Cell Biol 12 (2010) 143–152. https://doi.org/10.1038/ncb2014.

[31] M.N. Wosczyna, C.T. Konishi, E.E. Perez Carbajal, T.T. Wang, R.A. Walsh, Q. Gan, M.W. Wagner, T.A. Rando, Mesenchymal Stromal Cells Are Required for Regeneration and Homeostatic Maintenance of Skeletal Muscle, Cell Reports 27 (2019) 2029-2035.e5. https://doi.org/10.1016/j.celrep.2019.04.074.

[32] V. Bolduc, A.R. Foley, H. Solomon-Degefa, A. Sarathy, S. Donkervoort, Y. Hu, G.S. Chen, K. Sizov, M. Nalls, H. Zhou, S. Aguti, B.B. Cummings, M. Lek, T. Tukiainen, J.L. Marshall, O. Regev, D. Marek-Yagel, A. Sarkozy, R.J. Butterfield, C. Jou, C. Jimenez-Mallebrera, Y. Li, C. Gartioux, K. Mamchaoui, V. Allamand, F. Gualandi, A. Ferlini, E. Hanssen, S.D. Wilton, S.R. Lamandé, D.G. MacArthur, R. Wagener, F. Muntoni, C.G. Bönnemann, A recurrent COL6A1 pseudoexon insertion causes muscular dystrophy and is effectively targeted by splice-correction therapies, JCI Insight 4 (2019) e124403. https://doi.org/10.1172/jci.insight.124403.

[33] J.S. Bredfeldt, Y. Liu, C.A. Pehlke, M.W. Conklin, J.M. Szulczewski, D.R. Inman, P.J. Keely, R.D. Nowak, T.R. Mackie, K.W. Eliceiri, Computational segmentation of collagen fibers from second-harmonic generation images of breast cancer, J. Biomed. Opt 19 (2014) 016007. https://doi.org/10.1117/1.JBO.19.1.016007.

[34] Q. Li, T. Zhang, Y. Pan, L.C. Ciacchi, B. Xu, G. Wei, AFM-based force spectroscopy for bioimaging and biosensing, RSC Adv. 6 (2016) 12893–12912. https://doi.org/10.1039/C5RA22841G.

[35] L. Puricelli, M. Galluzzi, C. Schulte, A. Podestà, P. Milani, Nanomechanical and topographical imaging of living cells by atomic force microscopy with colloidal probes, Review of Scientific Instruments 86 (2015) 033705. https://doi.org/10.1063/1.4915896.

[36] M. Offroy, A. Razafitianamaharavo, A. Beaussart, C. Pagnout, J.F.L. Duval, Fast automated processing of AFM PeakForce curves to evaluate spatially resolved Young modulus and stiffness of turgescent cells, RSC Adv. 10 (2020) 19258–19275. https://doi.org/10.1039/D0RA00669F.

[37] G. Rubí-Sans, A. Nyga, E. Rebollo, S. Pérez-Amodio, J. Otero, D. Navajas, M.A. Mateos-Timoneda, E. Engel, Development of Cell-Derived Matrices for Three-Dimensional *In Vitro* Cancer Cell Models, ACS Appl. Mater. Interfaces 13 (2021) 44108–44123. https://doi.org/10.1021/acsami.1c13630.

[38] K. Karkali, I. Jorba, D. Navajas, E. Martin-Blanco, Measuring ventral nerve cord stiffness in live flat-dissected Drosophila embryos by atomic force microscopy, STAR Protocols 3 (2022) 101901. https://doi.org/10.1016/j.xpro.2022.101901.

[39] C. Jimenez-Mallebrera, M.A. Maioli, J. Kim, S.C. Brown, L. Feng, A.K. Lampe, K. Bushby, D. Hicks, K.M. Flanigan, C. Bonnemann, C.A. Sewry, F. Muntoni, A comparative analysis of collagen VI production in muscle, skin and fibroblasts from 14 Ullrich congenital muscular dystrophy patients with dominant and recessive COL6A mutations, Neuromuscular Disorders 16 (2006) 571–582. https://doi.org/10.1016/j.nmd.2006.07.015.

[40] S. Paco, T. Casserras, M.A. Rodríguez, C. Jou, M. Puigdelloses, C.I. Ortez, J. Diaz-Manera, E. Gallardo, J. Colomer, A. Nascimento, S.G. Kalko, C. Jimenez-Mallebrera, Transcriptome Analysis of Ullrich Congenital Muscular Dystrophy Fibroblasts Reveals a Disease Extracellular Matrix Signature and Key Molecular Regulators, PLoS ONE 10 (2015) e0145107. https://doi.org/10.1371/journal.pone.0145107.

[41] W.W. Chan, F. Yu, Q.B. Le, S. Chen, M. Yee, D. Choudhury, Towards Biomanufacturing of Cell-Derived Matrices, International Journal of Molecular Sciences 22 (2021) 11929. https://doi.org/10.3390/ijms222111929.

[42] G. Rubi□Sans, O. Castaño, I. Cano, M.A. Mateos□Timoneda, S. Perez□Amodio, E. Engel, Engineering Cell□Derived Matrices: From 3D Models to Advanced Personalized Therapies, Adv Funct Materials 30 (2020) 2000496. https://doi.org/10.1002/adfm.202000496.

[43] C. Júnior, A. Ulldemolins, M. Narciso, I. Almendros, R. Farré, D. Navajas, J. López, M. Eroles, F. Rico, N. Gavara, Multi-Step Extracellular Matrix Remodelling and Stiffening in the Development of Idiopathic Pulmonary Fibrosis, Int J Mol Sci 24 (2023) 1708. https://doi.org/10.3390/ijms24021708.

[44] P. Bonaldo, Collagen VI deficiency induces early onset myopathy in the mouse: an animal model for Bethlem myopathy, Human Molecular Genetics 7 (1998) 2135–2140. https://doi.org/10.1093/hmg/7.13.2135.

[45] X. Di, X. Gao, L. Peng, J. Ai, X. Jin, S. Qi, H. Li, K. Wang, D. Luo, Cellular mechanotransduction in health and diseases: from molecular mechanism to therapeutic targets, Sig Transduct Target Ther 8 (2023) 1–32. https://doi.org/10.1038/s41392-023-01501-9.

[46] C.M. Kraning-Rush, C.A. Reinhart-King, Controlling matrix stiffness and topography for the study of tumor cell migration, Cell Adh Migr 6 (2012) 274–279. https://doi.org/10.4161/cam.21076.

[47] E. Castroflorio, A.J. Pérez Berná, A. López-Márquez, C. Badosa, P. Loza-Alvarez, M. Roldán, C. Jiménez-Mallebrera, The Capillary Morphogenesis Gene 2 Triggers the Intracellular Hallmarks of Collagen VI-Related Muscular Dystrophy, IJMS 23 (2022) 7651. https://doi.org/10.3390/ijms23147651.

[48] M. Eroles, F. Rico, Advances in mechanical biomarkers, J of Molecular Recognition 36 (2023) e3022. https://doi.org/10.1002/jmr.3022.

a) Production of patient CDMs:

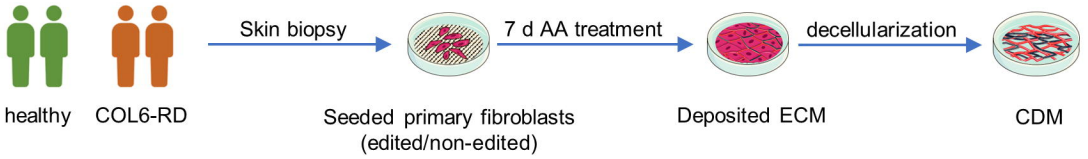

Gene editing. NAT for COL6-RD:

Mutation:

COL6A1 c.877G>A; p.Gly293Arg

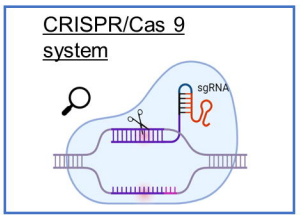

crRNA_1 = 5'-CCTGGTACCCAACAGGTCTG-3'

crRNA_2 = 5'-CCCGGGGACCTCAGACCTGT-3'

Non-homologous end joining

b) Immunofluorescence and CT-FIRE fiber analysis:

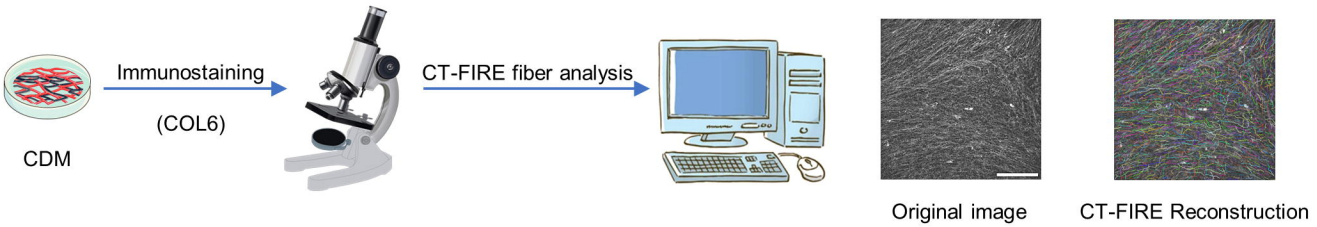

c) AFM-FS nanomechanical analysis:

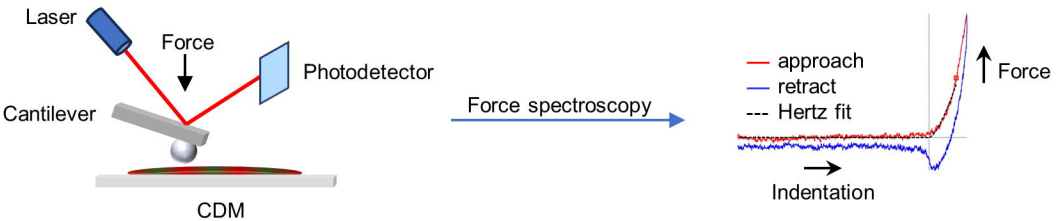

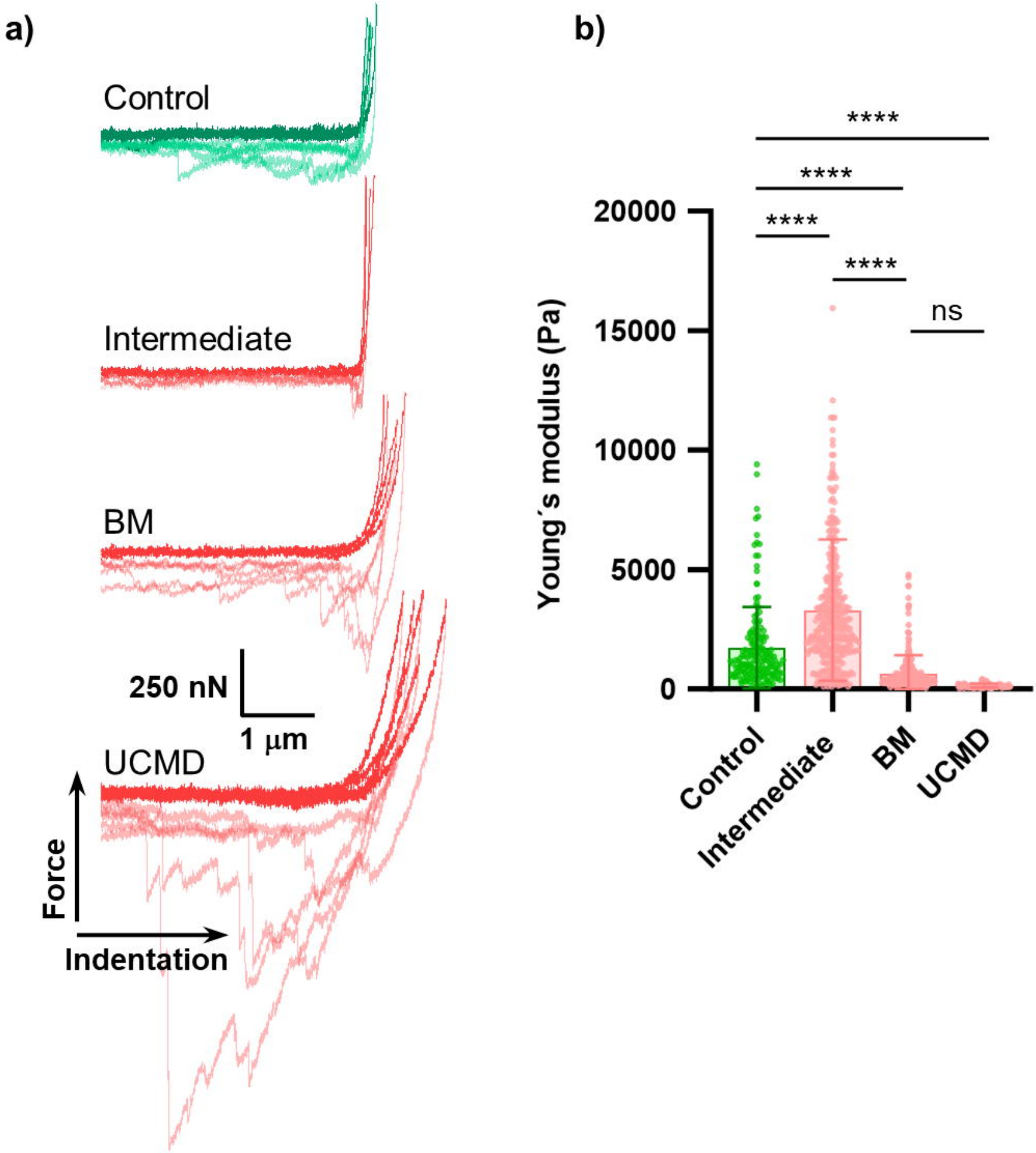
a)
Control
Intermediate
BM
UCMD
250 nN
1 µm
Force
Indentation
b)
Young´s modulus (Pa)
20000
15000
10000
5000
0
****
****
****
****
ns
Control
Intermediate
BM
UCMD

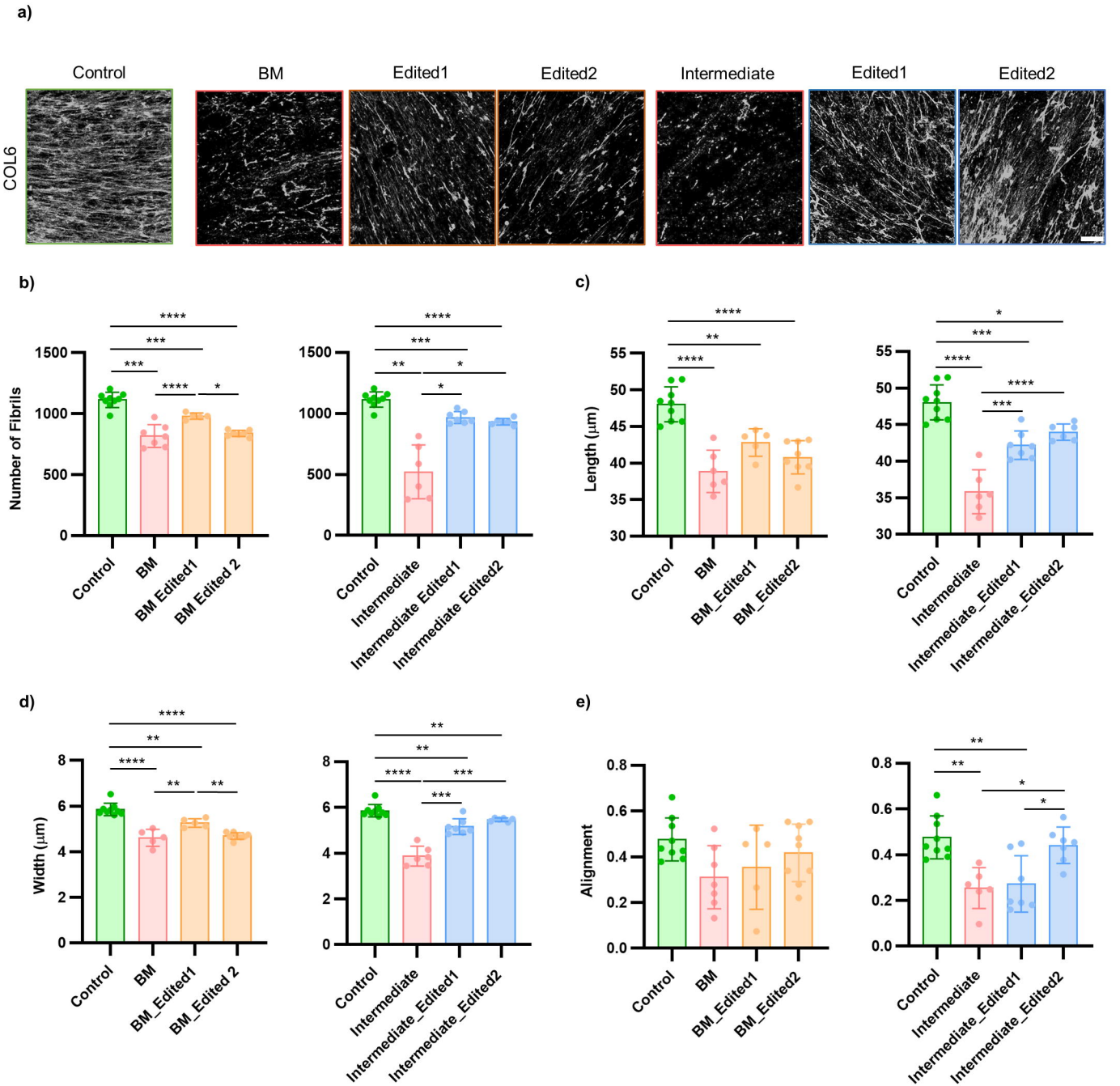
a)
Control
BM
Edited1
Edited2
Intermediate
Edited1
Edited2
COL6
b)
Number of Fibrils
Control
BM
BM Edited1
BM Edited 2
Intermediate
Intermediate Edited1
Intermediate Edited2
c)
Length (µm)
BM_Edited1
BM_Edited2
Intermediate_Edited1
Intermediate_Edited2
d)
Width (µm)
e)
Alignment

a)

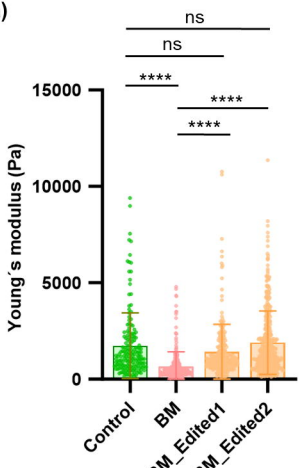
ns
ns
****
****
****
15000
10000
5000
0
Young´s modulus (Pa)
Control
BM
BM_Edited1
BM_Edited2

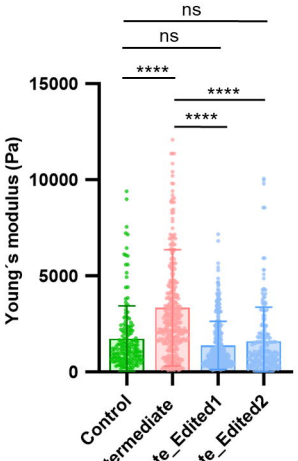
ns
ns
****
****
****
15000
10000
5000
0
Young´s modulus (Pa)
Control
Intermediate
Intermediate_Edited1
Intermediate_Edited2

b)

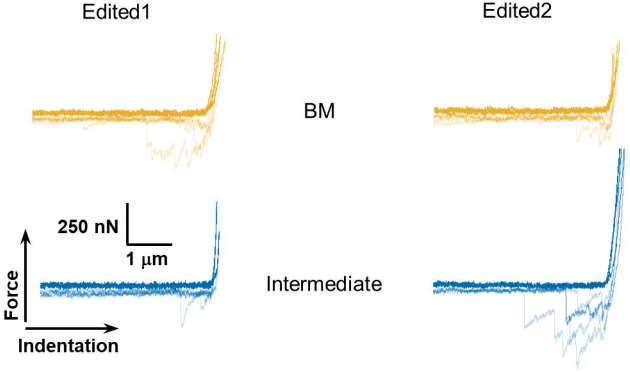
Edited1
Edited2
BM
Intermediate
250 nN
1 µm
Force
Indentation

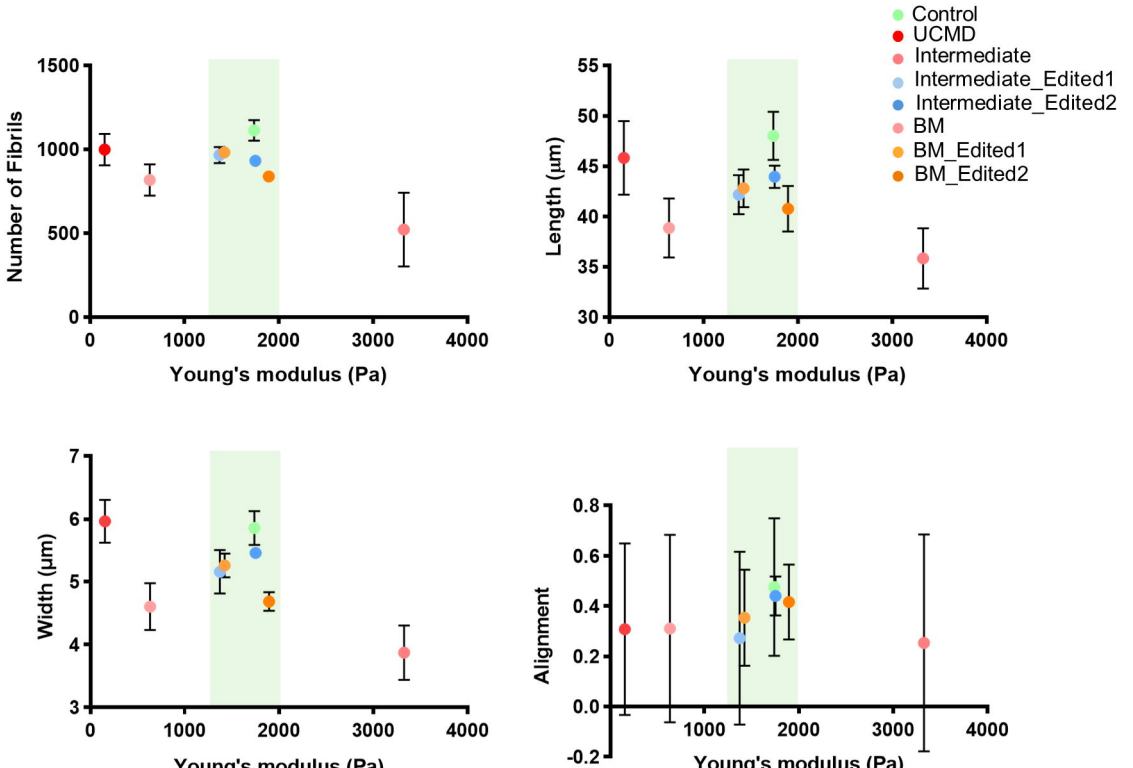
Control
UCMD
Intermediate
Intermediate_Edited1
Intermediate_Edited2
BM
BM_Edited1
BM_Edited2
Number of Fibrils
Length (µm)
Width (µm)
Alignment
Young's modulus (Pa)
Young's modulus (Pa)
Young's modulus (Pa)
Young's modulus (Pa)